CONTROL OF TWO-WHEELED INVERTED PENDULUM ROBOT USING ROBUST PI AND LQR CONTROLLERS

Tran Gia Khanh[1], Nguyen Hoai Nam[1,*], Tran Doan Xuan[2], Pham Tan Long[2], Trinh Duc Trung[3], Nguyen Doan Phuoc[1]

Abstract: *In this paper, a robust PI controller in combination with a linear quadratic regulator (LQR) is proposed to control a two-wheeled inverted pendulum robot (TWIPR) such that it is kept balanced while moving. The proposed TWIPR control system consists of two control loops. The inner loop has two PI controllers for two DC motors' currents, which are separately designed based on a robust PI controller structure. The outer loop contains a LQR controller for the tilt angle, heading angle and position of the TWIPR. The proposed PI controller is compared to the existing method such as the magnitude optimum (MO) and genetic algorithm (GA) methods. The proposed control scheme is verified through simulations and practical tests, and it is also compared to the MO-LQR and GA-LQR strategies.*

Keywords: PID tuning; DC motor control; Settling time; Overshoot; Two-wheeled inverted pendulum.

1. INTRODUCTION

TWIPRs were widely studied and applied in practice and literature [1-3]. The input to the TWIPR is usually torques produced by two DC motors. This torques is directly proportional to currents caused by the DC motors. Thus, the current controllers are crucial to the TWIPR. However, most of the works [4-19] about TWIPR have not addressed the problem of current or torque control. In addition, the voltages, applied to the DC motors, are considered as the input to the TWIPR instead of torques.

In [4], an adaptive back-stepping controller combined with two PD controllers was proposed for an electric scooter. The inputs to the vehicle were torques produced by two DC motors, but there was neither torque nor current controller designed. Sliding mode controllers with model-based friction compensation were proposed in [5] for a TWIPR. However, the torque/current control problem was also not dealt with. In [6], a nonlinear state transformation-based controller was proposed. A combination of two PD controllers and a time-delayed controller [7] for fast movement of TWMR was proposed, in which the first PD controller was designed for the pitch angle, the other PD controller was applied for the orientation, and the time delayed controller was synthesized for the position. In [8], the proposed control scheme consisted of local controller and a global planner for the TWIPR based personal transportation vehicle, in which the local controller contains three PID controllers for the pitch angle, the yaw angle and the position. Three fuzzy logic inference system-based controllers in [9] were designed for the TWIPR. In [10], an indirect adaptive fuzzy controller based on trajectory planner for the TWIPR was given. Adaptive sliding mode control [11] in combination with direct fuzzy control was applied for balancing and trajectory tracking of the TWIPR. A state dependent nonlinear model based LQR [12] was investigated. A back-stepping controller [13] was designed for trajectory tracking and sliding mode controllers were applied for the TWIPR's velocities and pitch angle. Four interval type 2 fuzzy logic inference system-based controllers [14] were designed using the Takagi-Sugeno model for the TWIPR such that the vehicle can reach the desired point and orientation while its balancing is kept. A passivity-based controller [15] with two-rule Takagi-Sugeno fuzzy model was proposed for the TWIPR. A novel TWIPR with four-bar parallel mechanism [16] developed, in which the horizontal posture was guaranteed. A model predictive controller [17] for the trajectory tracking of TWIPR was proposed. A trajectory planning and tracking control for obstacle avoidance of the TWIPR was given in [18]. A control of cooperative double-wheel inverted pendulum robots based on Udwadia-control approach was recently proposed in [19] for the first time. This motivates us to propose a new control strategy, which is simpler and effective in terms of installing the controller on microcontroller. In this work, a robust PI controller design method is proposed for the current of DC motor, then it is combined with a LQR controller to control the TWIPR, and finally it is compared with the other methods.

The next section presents the mathematical model and the proposed control system for the TWIPR. In section 3, robust PI controllers are designed for two DC motors' currents and they are compared to the MO and GA methods through simulations and experiments. In section 4, a LQR controller is designed to keep the TWIPR balanced and reach a desired position. Some simulations and practical tests for the TWIPR are given in section 5. The final section provides a summary and future works.

2. TWO-WHEELED INVERTED PENDULUM ROBOT

2.1. Mathematical Model

In this work, the mathematical model of TWIPR in [21] is used for simulation and controller design. The schematic diagram of a TWIPR is shown in fig. 1. The notations and parameters of the TWIPR are shown in Tab. 1, in which $J = mr^2/2$, $K = mr^2/4$, $I_1 = I_3 = Md^2/2$, $I_2 = Ml^2/2$. The inputs of the model [21] are torques produced by motors, but in this work, the two motors' currents are used instead of torques as the inputs to the TWIPR. Thus, the motion equations of the TWIPR are represented as in Eq. (1), (2) and (3).

$$m_{11}\ddot{x} - Ml\left(\dot{\psi}^2 + \dot{\theta}^2\right)sin\,(\theta) + m_{12}\ddot{\theta} + \frac{2}{C}\left(\frac{\dot{x}}{r} - \dot{\theta}\right) = \frac{K_m}{r}(i_L + i_R) \quad (1)$$

$$m_{21}\,\ddot{x} - m_{22}\ddot{\theta} + m_{23}\dot{\psi}^2 sin\,(2\theta) + g_2 - 2C\left(\frac{\dot{x}}{r} - \dot{\theta}\right) = -K_m(i_L + i_R) \quad (2)$$

$$m_{33}\ddot{\psi} + [Ml\dot{x} - m_{32}]\dot{\psi}\,sin\,(\theta) + \frac{C\dot{\psi}d^2}{(2r^2)} = \frac{(i_R - i_L)K_m d}{(2r)}, \quad (3)$$

where $m_{11} = M + 2m + \frac{2J}{r^2}$, $m_{12} = m_{21} = Mlcos\,(\theta)$, $m_{22} = (Ml^2 + I_2)$, $m_{23} = (I_3 - I_1 - Ml^2)/2$, $g_2 = -Mlgsin\,(\theta)$, $m_{32} = 2(I_3 - I_1 - Ml^2)$ and $m_{33} = I_3 + 2K + \frac{md^2}{2} + \frac{Jd^2}{2r^2} - (I_3 - I_1 - Ml^2)(\theta)$.

Let define state variables and inputs as

$$\underline{x} = [x_1\ x_2\ x_3\ x_4\ x_5\ x_6\ ]^T = \left[x\ \theta\ \psi\ \dot{x}\ \dot{\theta}\ \dot{\psi}\ \right]^T \quad (4)$$

and

$$\underline{u} = [u_1\ u_2\ ]^T = [i_L\ i_R\ ]^T, \quad (5)$$

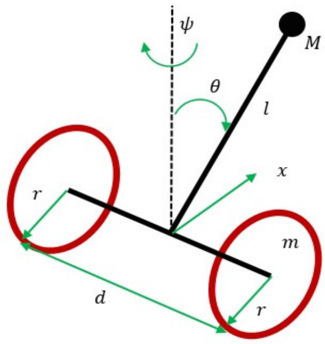

Figure 1. *Schematic diagram of a TWIPR.*

respectively. Then,

$$\underline{\dot{x}} = \underline{f}(\underline{x}, \underline{u}), \tag{6}$$

in which $\dot{x_1} = x_4$, $\dot{x}_2 = x_5$,$\dot{x_3} = x_6$, $\dot{x_4} = f_4(\underline{x}, \underline{u})$, $\dot{x_5} = f_5(\underline{x}, \underline{u})$ and $\dot{x_6} = f_6(\underline{x}, \underline{u})$, where $f_4(\underline{x}, \underline{u}) = \frac{\Omega_1+\Omega_2}{\Omega}$, $f_5(\underline{x}, \underline{u}) = \frac{\Omega_3+\Omega_4}{\Omega}$, and $f_6(\underline{x}, \underline{u}) = \frac{\Omega_5}{\Omega_6}$ with

$$\Omega_1 = r^2(Ml^2 + I_2)\left[\frac{K_m(u_1+u_2)}{r} + \frac{2C\left(x_5-\frac{x_4}{r}\right)}{r} + Mlsin\,(x_2)(x_5^2 + x_6^2)\right],$$

$$\Omega_2 = Mlr^2\cos(x_2)\left[m_{23}sin\,(2x_2)x_6^2 + K_m(u_1+u_2) + 2C\left(x_5 - \frac{x_4}{r}\right) + g_2\right],$$

$$\Omega_3 = m_{11}r^2\left[K_m(u_1+u_2) - m_{23}sin\,(2x_2)\,x_6^2 + 2C\left(x_5 - \frac{x_4}{r}\right) - g_2\right],$$

$$\Omega_4 = -Mlr^2cos\,(x_2)\left[\frac{K_m(u_1+u_2)}{r} + \frac{2C\left(x_5-\frac{x_4}{r}\right)}{r} + Mlsin\,(x_2)(x_5^2 + x_6^2)\right],$$

$$\Omega_5 = -2r^2\left(\frac{K_m(u_1-u_2)}{(2r)} + x_6sin\,(x_2)[Mlx_4 - 4m_{23}x_5cos\,(x_2)] + \frac{Cd^2x_6}{(2r^2)}\right),$$

$$\Omega_6 = (2I_3 + 4K + md^2 - 4m_{23}(x_2))r^2 + Jd^2, \text{ and}$$

$$\Omega = (Mlr)^2(1 - (x_2)) + 2I_2J + 2JMl^2 + (I_2M + 2I_2m + 2Mml^2)r^2.$$

Table 1. *TWIP's notations and parameters.*

Notation	Definition	Notation	Definition
x	Position of the TWIPR	K	MOI of the wheel w.r.t the vertical axis
θ	Pitch angle of the pendulum body	K_m	The motor torque constant
d	Distance from the left to right wheels	i_l, i_R	The left, right armature current
τ_L	Left motor's torque	τ_R	Right motor's torque
L	Length from the center of the pendulum to the wheel axis	C	Coefficient of viscous friction on wheel axis
J	Mass moment of inertia (MOI) of the wheel with respect to (w.r.t) the wheel axis	I_1	MOI of the pendulum w.r.t the frame at the center of the pendulum
M	Mass of the pendulum	M	Mass of left (right) wheel
ψ	Yaw angle of the TWIPR	R	Radius of wheels

The motion equations (1), (2), and (3) are used to design the LQR controller in Section 4. In the next section, PID controllers are designed to stabilize two motors' currents, which create desired inputs to the TWIPR.

2.2. TWIPR Control System

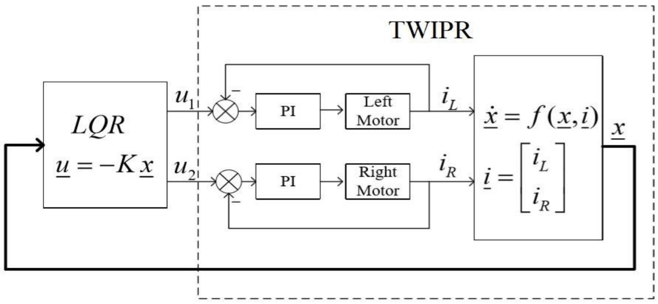

__Figure 2__. Block diagram of the TWIPR control system.

The block diagram of the proposed control strategy is shown in fig. 2. It contains three control loops, in which the first two inner loops consist of two PI controllers and the third loop has a LQR controller. A TWIPR in the laboratory are shown in fig. 3 and fig. 4.The TWIPR control system mainly consists of two DC motors, two current sensors INA219, two incremental encoders, two wheels, pendulum body, the MPU 6050 sensor, three batteries and the STM32F411VE MCU (powered by a 9V and 200mAh battery).

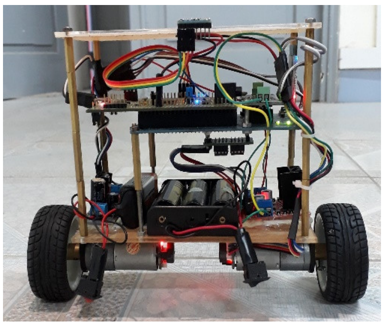

***Figure 3.** Front view of a TWIPR under control.*

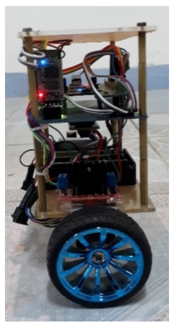

***Figure 4.** Side view of a TWIPR under control.*

2.2.1. DC Motor

Each DC motor has a gear chain with a gear ratio of n = 1/34. This means that the wheel, attached to the output shaft of the gear train, rotates n times for each revolution of the motor shaft. These two motors are powered by three 3.7V and 4000mAh batteries (Ultrafire).

2.2.2. Incremental Encoder

An encoder is also attached to each DC motor's rotor shaft. The encoder has two channels and each channel has $N = 13$ pulses per revolution of the motor. This incremental encoder is used with the highest resolution, so there are $4N/n = 1768$ pulses per revolution of the wheel. It is applied to measure both the angle and velocity of the wheel, then from these measurements, the position, heading angle, velocity and vertical speed of the TWMR are estimated.

2.2.3. Kalman Filter

In this subsection, the Kalman filter [22] is applied to estimate the tilt angle of the pendulum. Let ζ_k be the gyroscope signal from the *MPU6050* at k in time and ζ_k^{bias} be the deviation of ζ_k, and ΔT be the sampling time. Then, the tilt angle of the pendulum can be approximately calculated as

$$\theta_k = \theta_{k-1} + (\zeta_k - \zeta_k^{bias})\Delta \mathrm{T}. \tag{7}$$

Define state variables as $z_k = \left[\theta_k \;\; \zeta_k^{bias}\right]^T$. Then, the state space model is

$$z_k = A_\theta z_{k-1} + B_\theta u_k + w_k \tag{8}$$
$$\theta y_k = C_\theta z_k + v_k,$$

where $A_\theta = [1 \; -\Delta T;\; 0 \; 1]$, $B_\theta = [\,\Delta T \; 0\,]$, $C_\theta = [1 \; 0\,]$, $u_k = \zeta_k$, w_k is the input white noise, and v_k is the measurement white noise. Denote covariance matrices for w_k and v_k as Q_k and R_k, respectively.

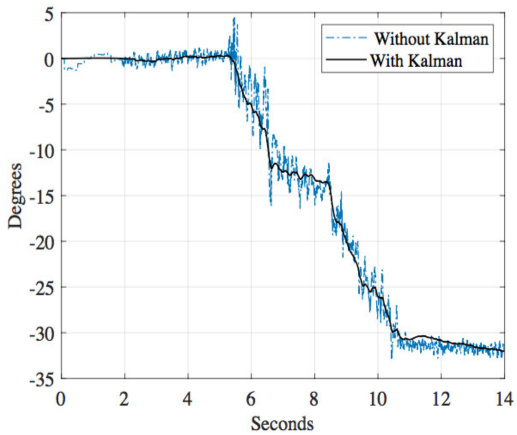

Figure 5. *Measured pitch angle with and without Kalman filter.*

Let $\hat{z}_k^-$ be the prior estimate, $e_{\underline{k}} = z_k - \hat{z}_k^-$ be the estimation error, and the corresponding error covariance matrix $P_{\underline{k}} = E\left[e_{\underline{k}}(e_{\underline{k}})^T\right]$. Then, the measurement $^{\theta}y_k$ will be used to improve the prior estimate as follows

$$\hat{z}_k = \hat{z}_k^- + K_k\left({}^{\theta}y_k - C_\theta \hat{z}_k^-\right), \tag{9}$$

where K_k is a Kalman gain (or blending factor) and $\hat{z}_k$ is the updated estimate. The Kalman gain is computed as

$$K_k = P_k^- C_\theta^T \left(C_\theta P_k^- C_\theta^T + R_k\right)^{-1}. \tag{10}$$

The covariance matrix with respective to the optimal estimate can be calculated as

$$P_k = (I - K_k C_\theta) P_k^-. \tag{11}$$

At time *k+1*,

$$\hat{z}_{k+1}^- = A_\theta \hat{z}_k + B_\theta u_k \tag{12}$$
$$P_{k+1}^- = A_\theta P_k A_\theta^T + Q_k.$$

Thus, the Kalman filter is implemented as the following steps:

Start with a prior estimate z_0 and its error covariance matrix P_0^-

• Step 1: Calculate the Kalman gain using Eq. (10).

• Step 2: Update estimate with measurement using Eq. (9)

• Step 3: Determine error covariance for updated estimate using Eq. (11).

• Step 4: Project ahead using Eq. (12), then goes back the first step.

This algorithm will be used to estimate the tilt angle of the pendulum based on the *MPU6050* sensor. In fig. 5, an example of the measured tilt angle is shown, where the black curve is the angle with Kalman filter and the blue curve is the angle without the filter.

3. CURRENT CONTROLLER DESIGN

3.1. Current Model Identification

In this section, the transfer function for the current of DC motors will be built using unit-step response. The electrical equation [23] for a DC motor is described as

$$u = e + Ri + L\frac{di}{dt}, \tag{13}$$

where u is the motor armature voltage, R is armature coil resistance, L is armature coil inductance, i is the armature current, $e = K_e\omega$ is the back electromotive-force voltage, ω is the motor angular speed, $\tau = K_m i$ is the motor torque, K_e is an electrical constant, and K_m is the motor torque constant.

Thus, the transfer function for the current of the motor is

$$G_i(s) = \frac{I(s)}{U(s)} = \frac{1}{R+Ls}, \text{ or} \tag{14}$$

$$G_i(s) = \frac{k}{Ts+1}, \tag{15}$$

where $k = 1/R$ and $T = L/R$.

To determine these parameters, a unit-step response approach is applied. A voltage of 6V is supplied to the motor, and then the motor's current is measured as shown in fig. 6. Based on this measured current, the current transfer function is obtained as follows

$$G_i(s) = \frac{0.13919}{1.23*10^{-4}s+1}. \tag{16}$$

From the identified model (16), the current controllers are designed with methods in the next section.

3.2. Robust PI Controller Design

Consider a plant as in Eq. (15). A PI controller is chosen as $R(s) = k_p(1 + \frac{1}{sT_i})$. Then, the closed-loop system is

$$G(s) = \frac{kk_p(sT_i+1)}{sT_i(Ts+1)+kk_p(sT_i+1)}. \tag{17}$$

Let $a = \frac{T_i}{T}$. Then, the characteristic equation is

$$aT^2s^2 + saT(1 + kk_p) + kk_p = 0. \tag{18}$$

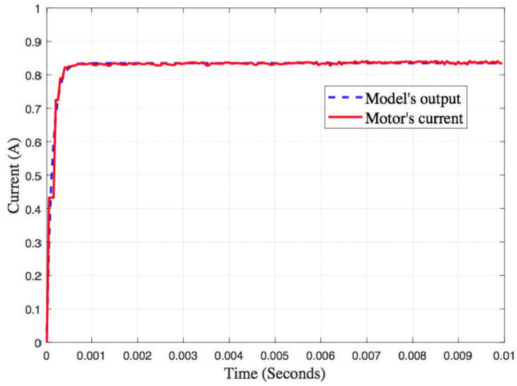

Figure 6*. Currents of motor and model current.*

Since all coefficients are positive, the closed-loop system is stable. Thus, the PI controller is robust in terms of structure. One has

$$\Delta = \left[aT\left(1+kk_p\right)\right]^2 - 4aT^2kk_p = (aT)^2\left[\left(1+kk_p\right)^2 - \frac{4kk_p}{a}\right], \tag{19}$$

so $\Delta \geq (aT)^2 4kk_p\left[1-\frac{1}{a}\right]$. Thus, if $a > 1$ then $\Delta > 0$, hence the two poles are negative. This means that there is no oscillation and zero overshoot. In addition, if $a = 1$, this is the case in [20], then $T_i = T$. The closed-loop system is

$$G(s) = \frac{RS}{1+RS} = \frac{1}{\frac{T_i}{kk_p}s+1}. \tag{20}$$

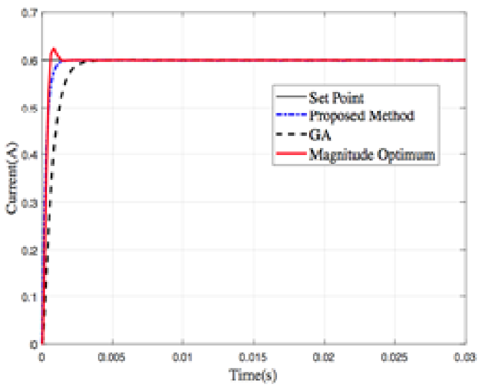

Figure 7*. Simulation results.*

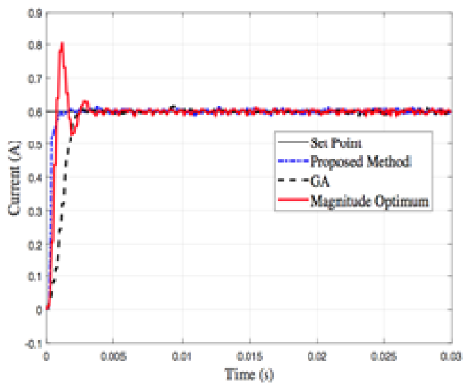

Figure 8*. Practical results.*

Consequently, the unit-step response is $h(t) = 1 - e^{-\frac{kk_p}{T_i}t}$. Let $T_{a\%}$ is the desired settling time of the closed-loop system, then

$$k_p = \frac{-T_i \ln\frac{a}{100}}{kT_{a\%}} \tag{21}$$

With these selections of PI parameters, there is no overshoot and the desired settling time is achieved as expected. For the plant (16), the desired settling time is chosen as $T_{a\%} = 1ms$. Thus, the parameters of the PI controller are computed as $k_P = 3.4563$ and $T_I = 1.23*10^{-4}$. As the magnitude optimum method [24] is applied for the current object, the parameter of the I controller $R_{mo}(s) = \frac{1}{T_i s}$ is calculated as $T_i = 2kT = 3.4232 * 10^{-5}$. The GA method [25] is also utilized to determine the current controller for the plant (16) using an objective function

$J = \int_0^{t_{final}} t|e(t)|dt \ \rightarrow min$. The GA based PI controller is obtained as $R_{ga}(s) = 0.064 + \frac{9936}{s}$.

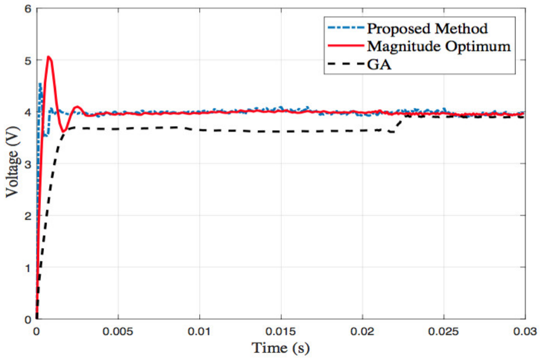

Figure 9. *Practical control signal.*

These controllers are utilized to control the motor's current. Both simulation and practical tests are carried out to compare the proposed method with the other methods as shown in fig. 7, 8 and 9. For simulation, Eq. (16) is used as the DC motor's current model and the PID controllers were designed above. In fig. 7, the controlled current is plotted via simulation. The proposed PI provides shorter settling time than the GA and MO methods. It also produces a zero overshoot as the GA method.

Table 2. *Comparison of methods through simulation and real test.*

Method	$T_{2\%}$ (ms)		Overshoot (%)	
	Simulation	Test	Simulation	Test
OSA	**1**	**1.1**	**0**	**1.36**
MO	1.04	3	4.32	29.92
GA	2.42	2.5	0	1

For experimental test, the DC motor given in section 2.2.1 (see fig. 3) was applied and its gear shaft is kept fixed, and the sampling time is 0.25 (ms). The practical result is shown in fig. 8, where the robust PI produces the best performance in comparison with the GA and MO methods. This will improve the control performance of the TWIPR. Fig. 9 shows the actual control signal (the applied voltage to the DC motor) produced by the di□erent controllers. The overshoot and settling time given by the controllers through both simulation and real test are compared in Tab. 2. Overall, the proposed PI controller is better than PID controllers using MO and GA methods in terms of both overshoot and settling time. In the next section, an LQR controller combined with the proposed PI controller is designed to keep the TWIPR balanced and follow desired trajectories.

4. LQR CONTROLLER DESIGN

4.1. Linearized Model of the TWIPR

Let $\underline{x}_e$ be an equilibrium point of the system (6), then $\underline{x}_e$ is the solution to the equation $\underline{f}(\underline{x}, \underline{0}) = \underline{0}$. Thus, $\underline{x}_e = [* \ \ 0 \ \ * \ \ 0 \ 0 \ 0\,]^T$ where '*' are any values of x_1 and x_3, which are desired position and heading angle of the TWIPR. Without loss of generality, it is assumed that '$*$' is zero, this means $\underline{x}_e = \underline{0}$. Thus, the linearized model of the system (6) around the equilibrium point x_e can be obtained as follows

$$\dot{\underline{x}} = A\underline{x} + B\underline{u}, \tag{22}$$

where

$$A = \begin{bmatrix} 0 & 0 & 0 & 1 & 0 & 0 \\ 0 & 0 & 0 & 0 & 1 & 0 \\ 0 & 0 & 0 & 0 & 0 & 1 \\ 0 & a_{42} & 0 & a_{44} & a_{45} & 0 \\ 0 & a_{52} & 0 & a_{54} & a_{55} & 0 \\ 0 & 0 & 0 & 0 & 0 & a_{66} \end{bmatrix} \tag{23}$$

and

$$B = [0\ 0; 0\ 0; 0\ 0; b_{41}\ b_{42}; b_{51}\ b_{52}; b_{61}\ b_{62}], \tag{24}$$

with $a_{42} = \frac{-(Mgl)^2 g}{\Lambda}$, $a_{44} = \frac{-2C((Ml^2+I_2)+Mlr)}{\Lambda}$, $a_{45} = \frac{2Cr(Ml^2+I_2)+2CMl^2}{\Lambda}$, $a_{52} = \frac{Mgl(2J+Mr^2+2mr^2)}{\Lambda}$, $a_{54} = \frac{2CMl+2C(2J+Mr^2+2mr^2)/r}{\Lambda}$, $a_{55} = \frac{2C(2J+Mr^2+2mr^3)+2CMlr}{-\Lambda}$, $a_{66} = \frac{-Cd^2}{2Jd^2+(2I_3+4K+md^2)r^2}$, $b_{41} = b_{42} = \frac{K_m r[(Ml^2+I_2)+Mlr]}{\Lambda}$, $b_{51} = b_{52} = \frac{-K_m(2J+Mr^2+2mr^2+Mlr)}{\Lambda}$, $b_{61} = -b_{62} = \frac{-K_m dr}{Jd^2+(2I_3+4K+d^2m)r^2}$, and $\Lambda = 2I_2J + 2JMl^2 + I_2Mr^2 + 2I_2mr^2 + 2Ml^2mr^2$.

4.2. LQR Controller

From the linearized model (22), a LQR controller [26] is designed such that the following cost function is minimized.

$$F = \int_0^\infty \left(\underline{x}^T Q_c \underline{x} + \underline{u}^T R_c \underline{u}\right) dt \to min, \tag{25}$$

in which Q_c is a symmetric positive definite matrix, and R_c is a symmetric nonnegative definite matrix. The controller, which satisfies the cost function (25), is $\underline{u} = -K_{LQR}\underline{x}$, where

$$K_{LQR} = R_c^{-1} B^T P_c, \tag{26}$$

and P_c is the solution to the Riccati equation

$$P_c B R_c^{-1} B^T P_c - P_c A - A^T P_c = Q_c. \tag{27}$$

In this paper, the values of the TWIPR's parameters are determined from a real TWIPR as follows *M = 0.5kg*, *m = 0.04kg*, *l = 0.08m*, *d = 0.16m*, *r = 0.033m*, *g = 9.81m/s*^{2}, *C = 0.005*, K_m *= 0.41202Nm/A*. Thus, the matrix *B* is

$$B = [0\ 0; 0\ 0; 0\ 0; 55.5\ 55.5;\ -548.6\ -548.6;\ -138.9\ 138.9\ ], \tag{28}$$

and the matrix *A* has the form as in Eq. (29) with $a_{42} = -11.4$, $a_{44} = -40.8$, $a_{45} = 1.35$, $a_{52} = 176.8$, $a_{54} = 403.4$, $a_{55} = -13.31$, $a_{66} = -8.1$.

$$A = \begin{bmatrix} 0 & 0 & 0 & 1 & 0 & 0 \\ 0 & 0 & 0 & 0 & 1 & 0 \\ 0 & 0 & 0 & 0 & 0 & 1 \\ 0 & a_{42} & 0 & a_{44} & a_{45} & 0 \\ 0 & a_{52} & 0 & a_{54} & a_{55} & 0 \\ 0 & 0 & 0 & 0 & 0 & a_{66} \end{bmatrix} \tag{29}$$

The matrices of the cost function are chosen as

$$Q_c = diag([4, 3, 2, 3.5, 0.001, 0.9\,]) \tag{30}$$

and

$$R_c = [1\ 0; 0\ 1\,]. \tag{31}$$

From Eq. (26) and Eq. (27), the gain matrix of the LQR controller is obtained as

$$K_{LQR} = \begin{bmatrix} -1.41 & -3.09 & -3.16 & -2.14 & -0.33 & -0.65 \\ -1.41 & -3.09 & 3.16 & -2.14 & -0.33 & 0.65 \end{bmatrix}. \tag{32}$$

The output of the LQR controller will be setpoint for the current controllers.

Remark 3. Since the input to the LQR controller consists of state variable pairs (x;$\dot{x}$), (θ;$\dot{\theta}$) and (ψ;$\dot{\psi}$), the LQR output is similar to the sum of the three PD controllers' output as in works [4, 7, 8], in which each state variable pair is the input to one PD controller.

Remark 4. The LQR controller in [12] is also compared to the state dependent LQR controller when the high yaw rate is considered.

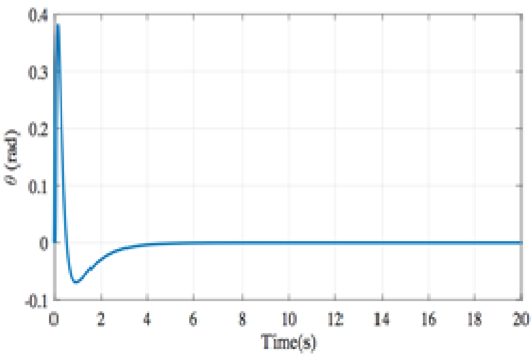

***Figure 10.** The tilt angle of the TWIPR through simulation.*

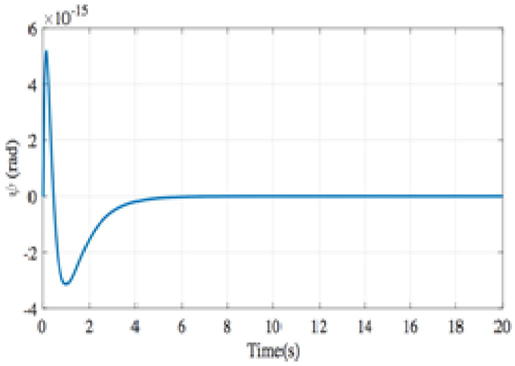

***Figure 11.** The heading angle of the TWIPR through simulation.*

5. SIMULATION AND PRACTICAL TEST

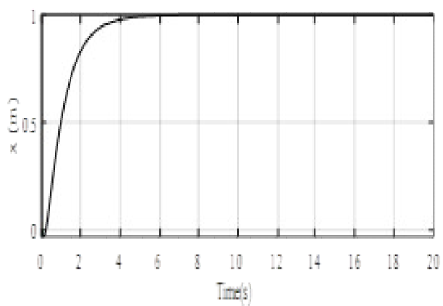

***Figure 12**. The position of the TWIPR through simulation.*

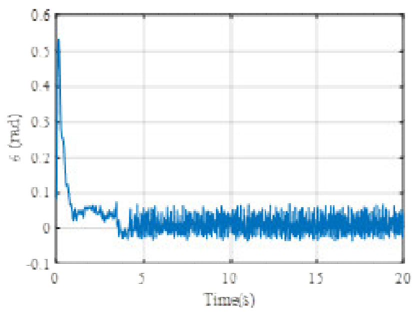

***Figure 13**. The tilt angle of the TWIPR through practical test.*

In this section, the proposed control scheme based on the robust PI design method and LQR controller is verified for the TWIPR through simulation and experiments. Then, it is compared to the other methods. The TWIPR is controlled to move from the initial point to the end point along a line, where the distance between these two points is *1* meter.

5.1. The proposed control strategy

The simulation results are shown in fig. 10, 11 and 12 whereas the experimental results are shown in fig. 13, 14 and 15. The left motor's measured current and right motor's measured current are shown in fig. 16 and 17. For simulation, the origin model as Eq. (6) and its parameters given in section 4.2 are applied for the TWIPR, in which the current control loops are modeled as saturation blocks since their settling time is very short 1 *(ms)*.

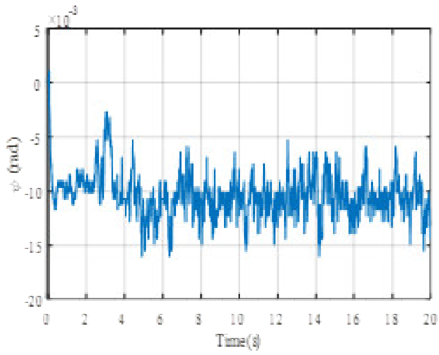

Figure 14. *The real heading angle of the TWIPR.*

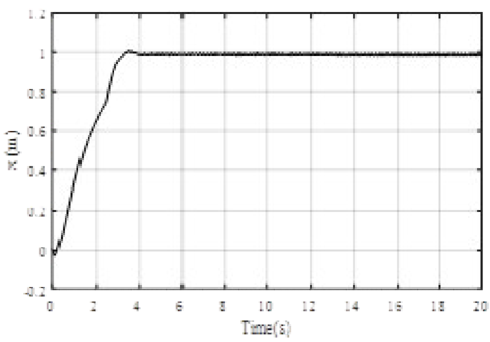

Figure 15. *The real position of the TWIPR.*

For experimental test, the sampling time for PID and LQR controllers is chosen as 0.25 (ms) and 2.5 (ms), respectively. From fig. 10 to fig. 15, it can be implies that the real-time results are similar to the simulation results. This implies that a good model of the TWIPR was built and the controllers work well. The proposed control strategy produces good performance such as the pitch angle lies within the interval $[-3\ 3]$ *(degrees)*, the TWIPR reaches the destination at 1 *(m)* after 3.5 *(seconds)* following a straight line because the yaw angle is approximately within the range $[-0.3\ 0.3]$ *(degrees)*.

5.2. Comparisons

The proposed control scheme based on the robust PI-LQR method is compared to the MO-LQR and GA-LQR methods through practical tests. The desired trajectory is a straight line with a length of 1 meter. Fig. 18 shows the positions of the TWIPR with different methods, where the blue curve, the black curve and the red curve are positions of the TWIPR provided by the proposed method, the MO-LQR method and the GA-LQR method, respectively.

The comparison of the pitch and yaw angles of the TWIPR with different methods are shown in fig. 19 and fig. 20, respectively. Since the yaw angles are very small for all methods, the TWIPR moves nearly along the straight line with distance of 1 meter. The robust PI-LQR based TWIPR moves more smoothly from the start point *0* to the end point with smaller pitch angle and less oscillation than the other methods. Hence, the proposed controller provides better performance than the others.

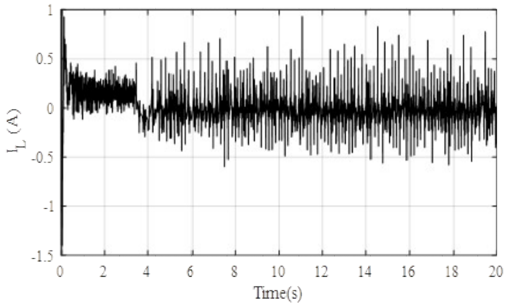

Figure 16. *Left motor's real current.*

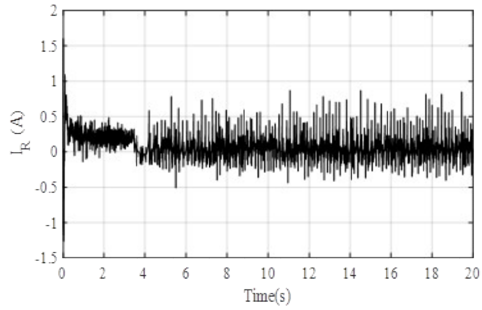

Figure 17. *Right motor's real current.*

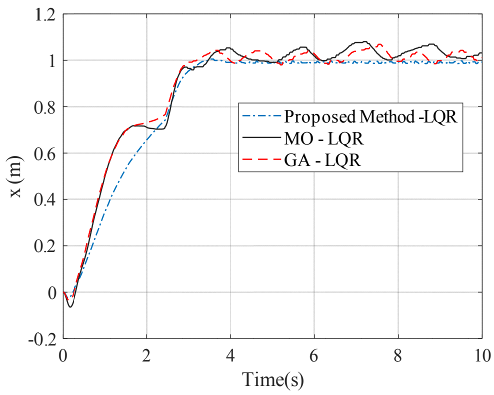

Figure 18. *The position of the TWIPR with different methods.*

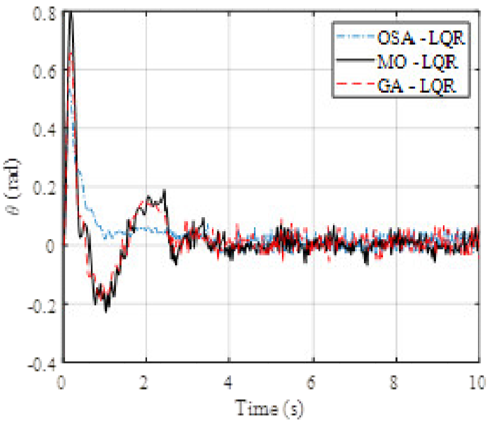

Figure 19. *The pitch angle of the TWIPR with different methods.*

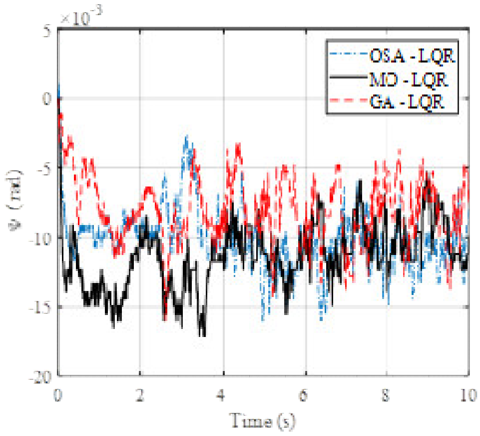

Figure 20. *The yaw angle of the TWIPR with different methods.*

Remark 5: The proposed control scheme is also tested with different loads and inclined surfaces. The practical results prove that the TWIPR is kept balanced and movable. However, they are skipped to show here.

6. CONCLUSIONS

In this work, the TWIPR control system based on the robust PI controller design method is proposed. First, the proposed method is compared to the MO and GA methods through the DC motor's current. It produces better performance than the others. Then, the proposed control system is verified and compared to the other methods through simulations and practical tests. The obtained results show that the TWIPR with the proposed method is kept balanced and able to reach the desired position and direction, and it produces better performance than the others. Future works will focus on the combination of the proposed method with other advanced control methods for the TWIPR.

Acknowledgement: *This research is funded by the Hanoi University of Science and Technology (HUST) under project number T2018-PC-052.*

REFERENCES

[1]. A. L. Cullen, "*A new free-wave method for ferrite measurements at millimeter wavelengths*," Radio Science, **Vol. 22**, pp. 1168-1170, (1987).

[2]. L. Zhijun, Y. Chenguang, and F. Liping, "*Advanced Control of Wheeled Inverted Pendulum Systems*," Springer, 280, (2013).

[3]. P. M. C. Ronald, A. S. Karl, and H. Roger, "*Review of modeling and control of two-wheeled robots*," Annual Reviews in Control, **Vol. 37**, pp. 89-103, (2013).

[4]. T. G. Khanh, N. D. Phuoc, and N. H. Nam, "*Advanced control methods for two-wheeled mobile robots*," The proceedings of the International Conference on System Science and Engineering. Ho Chi Minh, Vietnam, (2017).

[5]. N. N. Son and P. H. H. Anh, "*Adaptive Back-stepping Self-balancing Control of a Two-wheel Electric Scooter,*" Int. Jour. Advan. Robo. Syst., **Vol. 11**, pp. 1–11, (2014).

[6]. D. Fuquan, G. Xueshan, J. Shigong, G. Wenzeng, and L. Yubai, "*A two-wheeled inverted pendulum robot with friction compensation*," Mechatronics **Vol. 30**, pp. 116–125. (2015).

[7]. R. M. Brisilla and V. Sankaranarayanan, "*Nonlinear control of mobile inverted pendulum*," Robotics and Autonomous Systems, **Vol. 70**, pp. 145–155, (2015).

[8]. T. C. Sung and J. Seul, "*Combining Two Control Techniques for the Fast Movement of a Two-Wheel Mobile Robot*," Int. J. Human. Robot, **Vol. 12**, pp. 1–14, (2015).

[9]. H. W. Kim and S. Jung, "*Control of a two-wheel robotic 300 vehicle for personal transportation*," Robotica, **Vol. 34**, pp. 1186– 1208, (2016).

[10]. O. Akos, B. Ervin, K. Istvan, F. Janos and O. A. Peter, *Fuzzy Control of a Two-Wheeled Mobile Pendulum System*," Proceedings of the 11th IEEE Int. Symp. Appl. Comp. Intel. and Infor., Romania, (2016).

[11]. Y. Ming, A. Cong, D. Yu and S. Jianzhong, "*Indirect adaptive fuzzy control for a nonholonomic/underactuated wheeled inverted pendulum vehicle based on a data-driven trajectory planner*," Fuzzy Sets and Systems, **Vol. 290**, pp. 158–177, (2016).

[12]. Y. Ming, W. Shuang and S. Jian-Zhong, "*Simultaneous balancing and trajectory tracking control for two-wheeled inverted pendulum vehicles: A composite control approach,*" Neurocomputing **Vol. 191**, pp.44–54, (2016).

[13]. K. Sangtae and K. SangJoo, "*Nonlinear Optimal Con315 trol Design for Underactuated Two-Wheeled Inverted Pendulum Mobile Platform*," IEEE/ASME Transactions on Mechatronics, **Vol. 22**, pp. 2803 – 2808, (2017).

[14]. N. Esmaeili, A. Alireza and K. Hossein, "*Balancing and Trajectory Tracking of Two-Wheeled Mobile Robot Using Backstepping Sliding Mode Control: Design and Experiments,*" Journal of Intelligent and Robotic Systems, **Vol. 83**, pp. 601–613, (2017).

[15]. H. Jian, H. R. Myong, W. Dongrui and R. Songhyok, "*Interval Type-2 Fuzzy Logic Modeling and Control of a Mobile Two-Wheeled Inverted Pendulum*," IEEE Transactions on Fuzzy Systems, **Vol. 26**, pp. 2030–2038, (2018).

[16]. L. Rongjun, W. Junfeng, W. Dan, "*Sampled-data Fuzzy Control of Two-wheel Inverted Pendulums Based on Passivity Theory,*" International Journal of Control, Automation and Systems, **Vol. 16**, pp. 2538-2548, (2018).

[17]. J. Seonghee and H. Taisei, "*Development of a wheeled inverted pendulum mobile platform with a four-bar parallel mechanism*," Advanced Robotics, **Vol. 32**, pp. 1–11, (2018).

[18]. Y. Ming, A. Cong and S. Jian-Zhong, "*An Efficient Model Predictive Control for Trajectory Tracking of Wheeled Inverted Pendulum Vehicles with Various Physical Constraints*," International Journal of Control, Automation and Systems, **Vol. 16**, pp. 265–274, (2018).

[19]. N. Yigao, Y. Ming, Y. Lu and H. Xiaoqiang, "*A trajectory planning and tracking control approach for obstacle avoidance 340 of wheeled inverted pendulum vehicles,*" International Journal of Control, https://doi.org/10.1080/00207179.2018.1530455 (2018).

[20]. H. Chunsheng, H. Kang, C. Xiaolong, Z. Yiran and Z. Han "*Transportation control of cooperative double-wheel inverted pendulum robots adopting Udwadia-control approach*," Nonlinear Dynamics, **Vol. 91**, pp. 2789–2802, (2018).

[21]. N. H. Nam and N. D. Phuoc, "*Overshoot and settling time assignment with pid for first order and second-order systems,*" IET Control Theory and Applications, **Vol. 12**, pp. 2407– 2416, (2018).

[22]. K. Sangtae and K. SangJoo, "*Dynamic Modeling of a Two-wheeled Inverted Pendulum Balancing Mobile Robot*," International Journal of Control, Automation, and Systems, **Vol. 13,** pp. 926–933, (2015).

[23]. G. B. Robert and Y. C. H. Patrick, "*Introduction to Random Signals and Applied Kalman Filtering with Matlab Exercises*," Fourth Edition, John Wiley and Sons, Inc, (2012).

[24]. P. Jinzhu and D. Rickey, "*Identification and adaptive neural network control of a DC motor system with dead-zone characteristics*," ISA Transactions, **Vol. 50**, pp. 588–598, (2011).

[25]. W. U. Jeffrey and S. Mohammed, "*Magnitude and symmetric optimum criterion for the design of linear control systems: What is it and how does it compare with the others?*," IEEE Trans. Indus. Appl., **Vol. 26**, pp. 489–497, (1990).

[26]. T. Neenu and P. Poongodi, "*Position Control of DC Motor Using Genetic Algorithm Based PID Controller*," Proc. Worl. Cong. Engineering, London UK, pp. 1–5, (2009).

[27]. D. O. A. Brian and B. M. John, "*Optimal Control: Linear Quadratic Methods*," Prentice-Hall International, Inc, (1989).
[28]. T. G. Khánh, L. V. Anh, P. A. Tuấn, P. X. Minh, N. H. Nam, "*Điều khiển xe hai bánh tự cân bằng mô hình bất định dựa trên phương pháp quy hoạch động thích nghi*," The 1st National Conference on Dynamics and Control, Danang, Vietnam, (2019).
[29]. N. V. Khanh, T. T. Hùng, "*Điều khiển thời gian thực robot hai bánh tự cân bằng sử dụng bộ điều khiển PID mờ tự chỉnh,*" Hội nghị toàn quốc lần thứ 3 về Điều khiển và Tự động hoá, (2015).
[30]. N. M. Tâm, N. V. Đ. Hải, N. P. Lưu, L. V. Tuấn, "*Mô hình hóa và điều khiển tối ưu cho hệ xe hai bánh tự cân bằng,*" Đại học Sư phạm Kỹ thuật Hồ Chí Minh, (2017).
[31]. A. N. K. Nasir, M. A. Ahmad, R. M. T. Raja Ismail, "*The Control of a Highly Nonlinear Two-wheels Balancing Robot: A Comparative Assessment between LQR and PID-PID Control Schemes,*" WASET International Journal of Mechanical and Mechatronics Engineering, **Vol. 4**, (2010).
[32]. A. Y. Zimit, H. J. Yap, M. F. Hamza, I. Siradjuddin, B. Hendrik, T. Herawan, "*Modeling and Experimental Analysis Two-Wheeled Self Balance Robot Using PID Controller,*" Lecture Notes in Computer Science, **Vol. 10961**, Springer, Cham, (2018).

TÓM TẮT

ĐIỀU KHIỂN XE HAI BÁNH CÂN BẰNG SỬ DỤNG BỘ ĐIỀU KHIỂN PI BỀN VỮNG VÀ LQR

Trong bài báo này, một bộ điều khiển PI bền vững kết hợp với bộ điều khiển LQR được đề xuất để điều khiển xe hai bánh sao cho xe thẳng bằng khi di chuyển. Hệ thống điều khiển gồm hai vòng. Vòng trong có hai bộ điều khiển dòng PI để điều khiển dòng động cơ một chiều, được thiết kế riêng sử dụng cấu trúc PI bền vững. Vòng ngoài có bộ điều khiển LQR cho góc nghiêng, góc hướng và vị trí xe. Phương pháp thiết kế bộ điều khiển PI đề xuất được so sánh với phương pháp tối ưu độ lớn và giải thuật di truyền. Cấu trúc điều khiển đề xuất được kiểm chứng thông qua mô phỏng và thực nghiệm, và nó được so sánh với các phương pháp MO-LQR và GC-LQR.

Từ khóa: Chỉnh định PID; Xe hai bánh; Điều khiển động cơ; Thời gian xác lập.

Received 02nd March 2020
Revised 14th April 2020
Published 06th May 2020

Author affiliations:
[1]Hanoi University of Science and Technology, No. 1, Dai Co Viet Street, Hanoi, Vietnam;
[2]Viện Hàng không Vũ trụ Viettel;
[3]Công ty Ô tô Toyota Việt Nam.
[*]Corresponding author: nam.nguyenhoai@hust.edu.vn.